KLOE MEMO n^o 282
December 2005

Precise measurement of the η mass.

B. Di Micco

Università degli Studi di Roma Tre
I.N.F.N sezione di Roma III

Abstract

An integrated luminosity of 410 pb^{-1} of KLOE data, corresponding to $\sim$ 17 million of η events from the $\Phi \to \eta\gamma$ radiative decay, have been analyzed to measure the η mass using the decay $\eta \to \gamma\gamma$. The signal is searched in events with 3 photons in the final state. To this aim we perform a kinematic fit imposing energy momentum conservation on the 3 γ system. As shown in the following, the η mass value is insensitive to the calorimeter energy calibration and the systematic error on the measurement is dominated by the knowledge of the I.P position and of the sqrt(s). The decay channel $\phi \to \pi^0\gamma, \pi^0 \to \gamma\gamma$ is used as a crosscheck of the method, comparing the π^0 mass obtained by this method with that reported in the PDG[7]. The result obtained is $m_\eta = 547.82 \pm 0.016_{stat.} \pm 0.050_{syst.}$, this represent today best measurement of the η mass. The value is in agreement with the NA48[3] and in disagreement with the GEM measurement [4] and the experiments performed before NA48.

1 Introduction

The η mass measurement has been performed using dfferent techiniques by several experiments in the history [7]. It was measured using hadron machine with different technique and several production reactions.
The most recent measurements start from 1974 in the Rutherford Laboratory that used the reaction $\pi^- p \to n$neutrals.
The neutron is detected and the measurement is based on the determination of the threshold of the cross section $\pi^- p \to \eta n$. The n is compelled in a kinematic region such that the missing mass of the neutral system is given by the momentum of the π^- beam missing mass determination of the neutrals system. The value obtained is $m_\eta = 547.45 \pm 0.25$ MeV/c^2[1]. In this measurement no estimate of systematic effects has been computed, because the η mass measurement was not the main

target of the experiment and it was just used as a guideline for detector resolution studies. A later measurement at SATURNE [2] used the threshold determination of the reaction $dp \rightarrow^3 He\eta$. The beam momentum at threshold was used to determine the η mass, and two reactions were needed in order to calibrate the beam momentum $dp \rightarrow^3 He\pi^+$ and $dp \rightarrow pd$, $dp \rightarrow pd$, they measure $m_\eta = 547.30 \pm 0.15$ MeV/c^2. The systematic effect considered include uncertainties on the target thickness and the structure of the dependence of the beam momentum as a function of time. Systematic effects due to the spectrometer performances (non linearity, absolute calibration and so on) are not mentioned in the article.

Again with threshold determination of the reaction $\gamma p \rightarrow \eta p$ the η mass was measured at the MAMI[5] accelerator with the TAPS experiment. The photons were produced by the brehmstrhalung of electrons on a radiator foils and the energy measured as the difference between the going out electron, measured in a spectrometer, and the incoming electron energy. The measurement rely on the determination of the η cross section measurement. The only effect considered in the systematic is the uncertainty on the e^- momentum due to the spectrometer calibration. No effect due to soft photons emission in the bremstrahlung process and detector efficiency are considered in the systematic. They measured $m_\eta = (547.12 \pm 0.06 \pm 0.25) MeV/c^2$.

The first very precise measurement was performed by the NA48 collaboration. The measurement was performed using the $\eta \rightarrow 3\pi^0$ decay. Small sensitvity to the calorimeter absolute scale was shown because the invariant mass was built using geometric positions of the clusters. Systematic due to detector non linearity, geometry distortion and detector response were carefully determined. Crosschecks were done using the $\eta \rightarrow \gamma\gamma$ decay and the same technique was used to determine the K_L mass from $K_L \rightarrow 3\pi^0$. The NA48 experiment measured $m_\eta = 547.843 \pm 0.030 \pm 0.041$[3], a value that is 0.6 MeV/c^2 higher than the average od the previous measurements and more than 5 σ away.

This situation triggered a new high precision measurement at the COSY facility by the GEM collaboration[4]. In this case, a missing mass technique was used to determine the η mass in the reaction $p + d \rightarrow^3 He + \eta$. The spectrometer was calibrated using other two reactions. Because the spectrometer setting was changed during the calibration procedure, it is not clear the validity of the calibration. The working point of the spectrometer was in fact changed. Also the systematic study doesn't take into account non linearity of the apparatus and doesn't discuss the systematic linked to the knowledge of the calibration parameters.A very important effect, that is the variation of the target thickness with the time, is not taken into account in the systematic error. The final result is $m_\eta = 547.311 \pm 0.028_{\rm stat} \pm 0.032_{\rm syst}$ MeV/c^2.

This last measurement is in disagreement with the NA48 measurement and agrees with the old experiment. The present situation is summarized in fig. 1.

The average of the not NA48 measurement is 547.298 ± 0.040 MeV/c^2. The discrepancy with NA48 is at 10 σ. Despite to the fact that the NA48 measurement seem more robust from the experimental point of view for the several cross checks

261.25

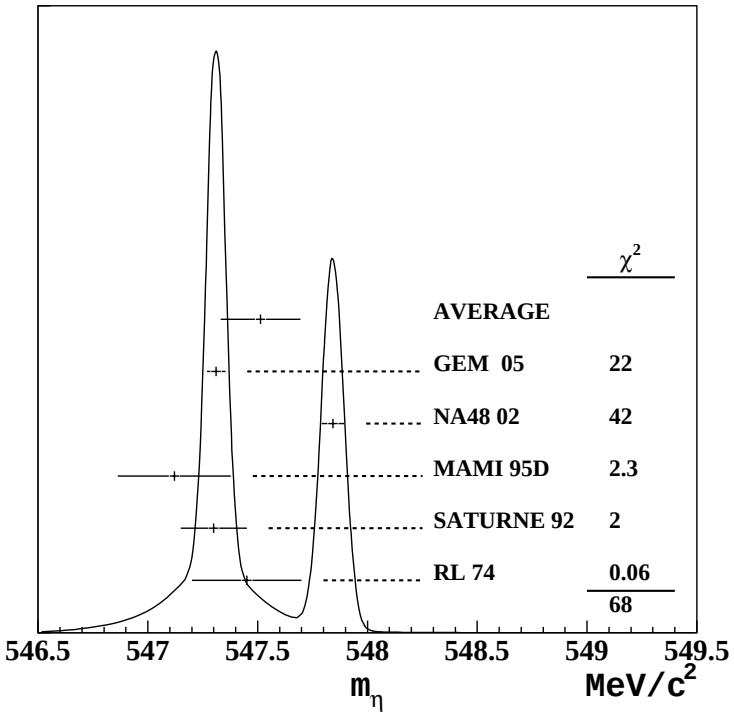

0

Figure 1: Eta mass measurement, see text for the references. The continuous line and the average has been computed using the PDG scheme [7].

performed and the agrrement of the K_L mass to the PDG value, the experimental situation now seems to invalidate the NA48 measurement. For this reason it is interesting that KLOE gives a measurement of the η mass in order to clarify the situation. Triggered by this problem at MAMI there is an ongoing experiment on the η mass measurement with an improved detector, that has a much better resolution on the measurement of the outgoing electron energy. [6].

The pourpouse of this work is to measure the η mass at 10 KeV level, in order to give a further measurement of this quantity to disentangle between the two last most precise measurements.

2 The method.

At KLOE a large number of η mesons is produced through the radiative ϕ decay $\phi \to \eta\gamma$. One of the main decay mode of the η meson is $\eta \to \gamma\gamma$. So the decay $\phi \to \eta\gamma$ produces three clusters in the calorimeter. In 2001+2002 the KLOE collected luminosity is about 450 pb^{-1} corresponding to 19 millions of η mesons and 7 millions of $\eta \to \gamma\gamma$ decays. The aim of this work is to measure the η mass at 2×10^{-5} level. This level of precision is unachievable with the calorimeter energy measurement due to the uncertainty in the calorimeter energy calibration. In fig. 2 the total energy of three photons events $\phi \to \eta, \pi^0\gamma$, $e^+e^- \to \gamma\gamma\gamma$ as a function of the run number is reported. The distribution on the right shows the total energy of the three most energetic photons on time impinging on the barrel in the angular region $50° < \theta_\gamma < 130°$. The peak at the ϕ mass is due to events coming from the ϕ decay into three photons, while the peak at a lower mass value is due to events with more than three photons where some photons are out of the angular range.

The plot shows a miscalibration of about 6 MeV on the total energy. So the miscalibration is at 6×10^{-3} level. Therefore the invariant mass of the two photons coming from the η cannot be used as it is to measure the η mass at 2×10^{-5}. Furthermore the calorimeter energy resolution is not enough to achieve the target.

In fig. 3 the invariant mass of 2 photons is reported for all combinations of two photons. The σ of the peak is 81 MeV/c^2, so we would need about 60 millions of events to reach the statistical precision of 10 keV.

The precision of the method is based on the fact that in a 3 photons system the energy momentum conservation impose 4 constraints to the photon kinematic.
The kinematic of the system is determined by the 3 energies of the 3 photons and by the 6 angles. Using the 4 constraints it is possible to express the energy in function of the 6 angles. This work is done by a kinematic fit with the following constraints:

- Total quadrimomentum of the three photons: P_x, P_y, P_z, E_{tot};
- $t_i - r_i/c = 0$ for each cluster i;

The procedure used for the fit is the same used for the $\eta \to 3\gamma$ upper limit determination [8]. The total quadrimomentum is determined by the **BMOM**, **BPOS**

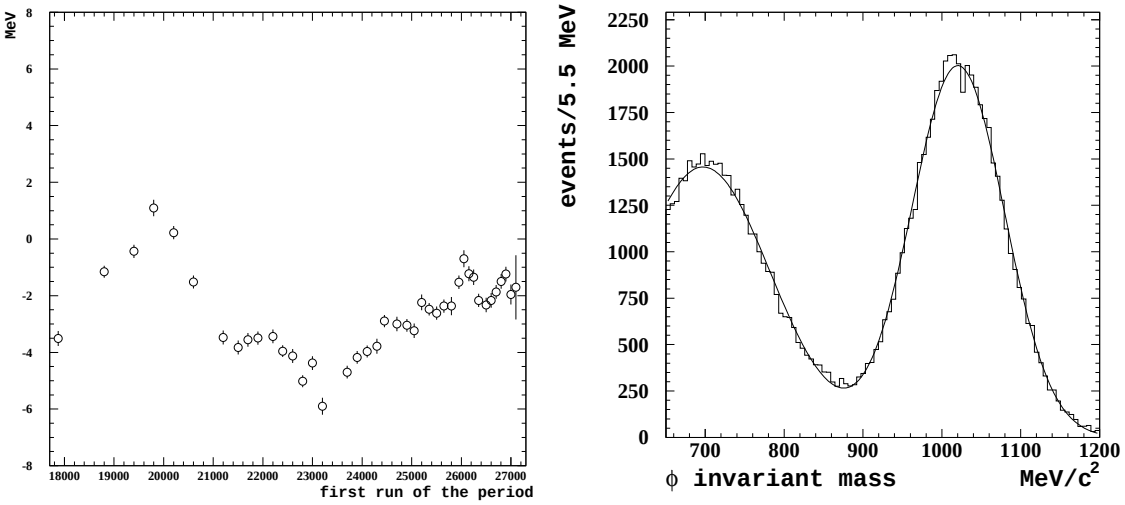

Figure 2: **left** Φ mass built from the energy of the three photons ($m_\phi = \sqrt{E_{\rm tot}^2 - P_x^2}$ as a function of the run period. Each point is about 10 pb^{-1} taken starting from the run on the abscissa; **right** distribution used to evaluate the invariant mass, the fit is done using a double gaussian model for the signal and the background.

algorithm [9] that studies the bhabha events to determine the mean vertex position X_v, Y_v, Z_v and the Φ boost.

The constraints on the time of the clusters, that is compatible with the time needed by a photon to travel the distance between the interaction point (i.p. in the following) and the cluster position, improves the resolution on the z coordinate and therefore on the angle of the photons.

In fig. 4 is the resolution σ_z as a function of the kine energy of the phtons. This distribution has been obtained by evaluating the difference between the reconstructed z of the cluster and the z position of the extrapolated point starting from the i.p. of the direction o the photons. An improvement of about 40% is obtained.

The effect of the kinematic fit can be appreciated in fig. 5. On the left side the combiantorial $m_{\gamma\gamma}$ distribution before the kineamtic fit is plotted, while on the right the same distribution after the kinematic fit is plotted. The huge improvement in the mass determination is evident.

3 Signal selection

The selection of the signal is very simple. Being the statistic not an issue we can require high quality events in order to reduce all systematic effects. After the usual

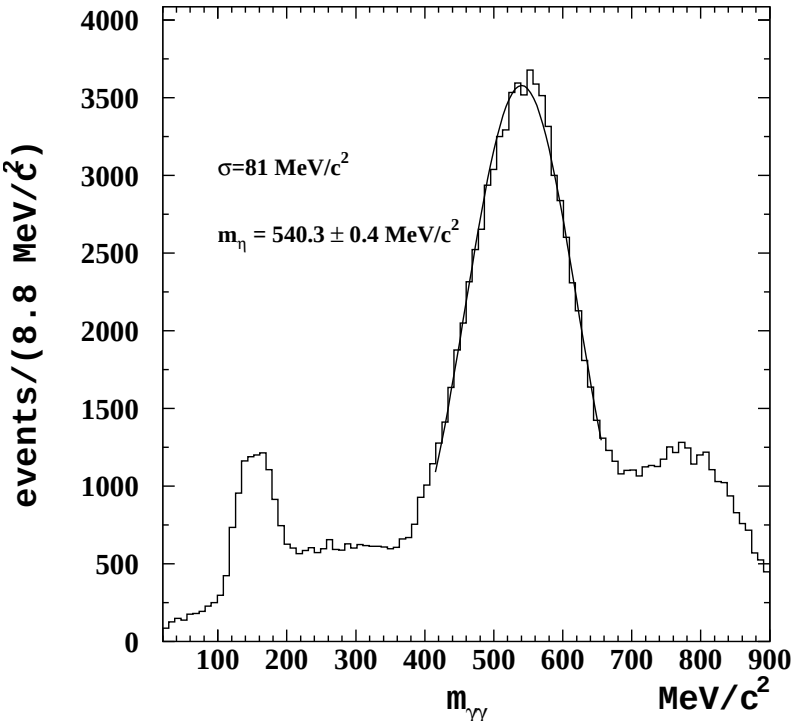

Figure 3: $m_{2\gamma}$ mass built using the energy and the cluster position, without any constraint on the total quadrimomentum.

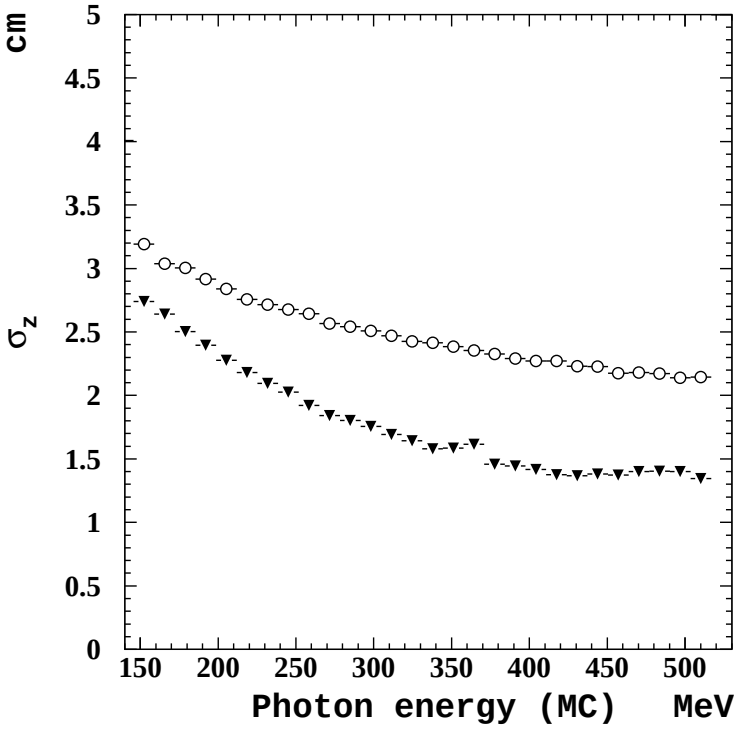

Figure 4: Resolution on the z coordinate of the photons as a function of the kine MC energy. The open circle is before the kinematic fit the full triangle is after the kinematic fit with $t - r/c$ constraint.

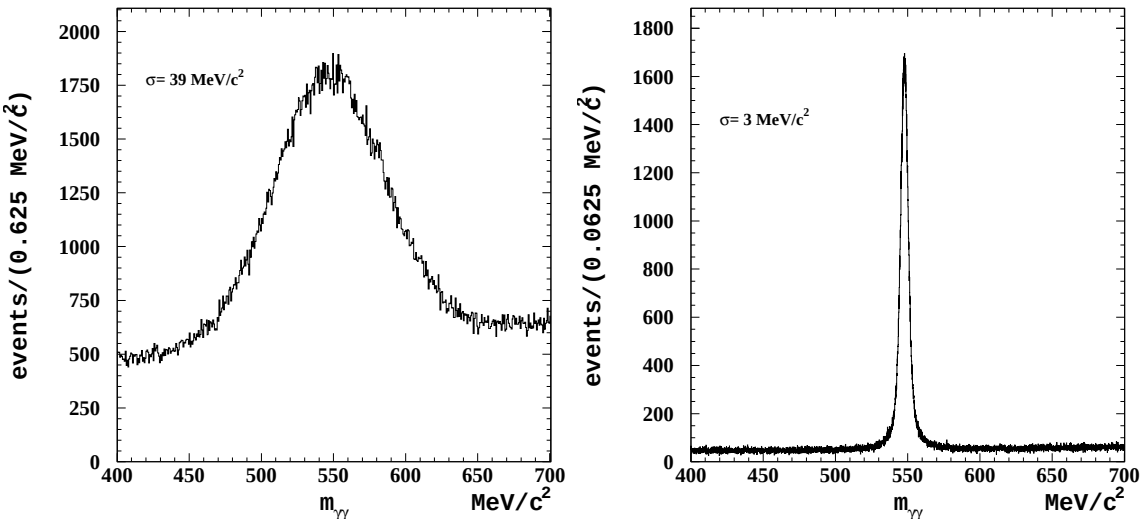

Figure 5: **(left)** m_η distribution built before the kinematic fit procedure, **(right)** the same after the kinematic fit.

FILFO,EVCL filter for the radiative stream we require at least three clusters whose time and position is compatible with the photon velocity:

$$|t - r/c| < min(5\sigma_t, 2\text{ns})$$

where σ_t is parametrized according the formula:

$$\sigma_t = \frac{5.4\%}{\sqrt{E(\text{GeV})}} \oplus 140\text{ps}$$

with angle $50°\theta_\gamma < 150\circ$.

Let's indicate with N_{pre} the number of clusters that survive this preselection. For each combination of three clusters of the total $\binom{N}{3}$ we compute the sum of the energy of the clusters E_{tot}, and we select the combinations with $E_{\text{tot}} > 650$MeV. To these the kinematic fit procedure is applied.

The loose cut is applied to reduce the number of combination on which the kinematic fit works, being an iterative procedure working on the linearization of the non linear constraints it is heavily cpu consuming. The selected combination are ordered by the χ^2 and the combination with the smallest χ^2 is retained as an effective three photons events.

A cut of $\chi^2 < 35$ is applied to reject background. The events rejected by this cut are events coming from events with $N_\gamma > 3$ or from events with $N_\gamma = 3$ but where one of the photons imps with an angle smaller than 50° on the calorimeter. In fig. 6 (left) the χ^2 distribution of the data and of the MC events with 3γ ($\phi \to \pi^0\gamma$, $\phi \to \eta\gamma$) is shown.

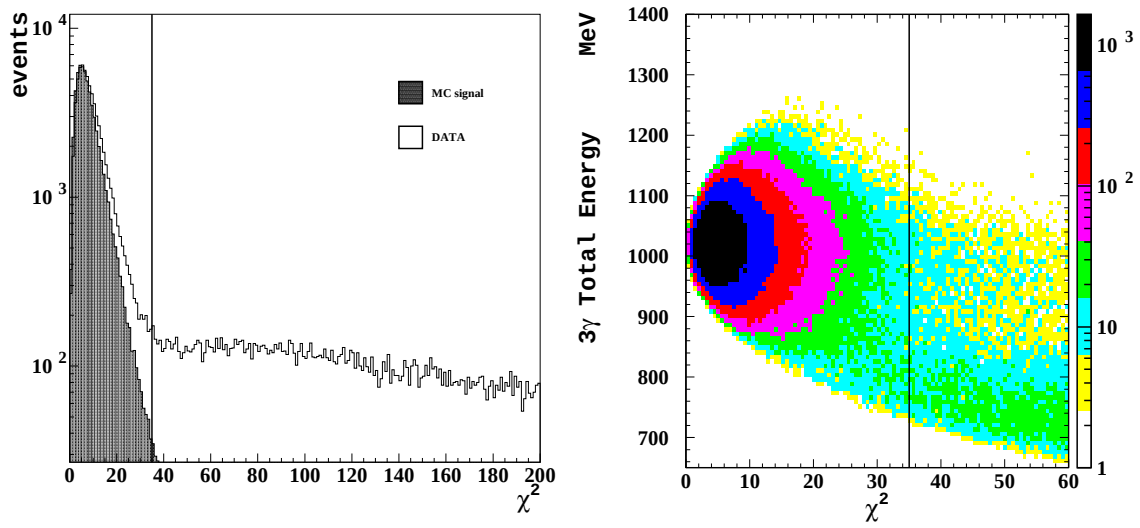

Figure 6: **(left)** χ^2 distribution for data and MC (3γ sampe), the cut used is shown; **(right)** Scatter plot of $E_{\rm tot}$ versus χ^2 on the DATA sample. The line shown refers to the cut used to select a clean sample of $\eta \to \gamma\gamma$ continuous line, and $\pi^0 \to \gamma\gamma$ dashed line.

In fig.6 (right) the scatter plot of $E_{\rm tot}$ as a function of th χ^2 is shown. It is evident that, given the cut $\chi^2 < 35$, the cut at 650 MeV is completely ineffective on the signal selection. The best way to show the mass distribution for the signal and the background, is to plot the dalitz plot of the 3 photons. Let's order the 3 γ according their energies $E_1 < E_2 < E_3$, and let's build the Dalitz plot using the variables $m^2 12$, m^2_{13}, the invariant masses of the pairs 1-2 and 1-3 respectively. In fig.7 these plots are shown for the data before and after the cut on the $\chi^2 < 35$.

Plotting $m_{\gamma 1 \gamma 2}$ variable we obtain the plot shown in fig.8 left. Two very narrow peaks are visible, the peak at the π^0 mass, due to the $\phi \to \pi^0\gamma$,$\pi^0 \to \gamma\gamma$ and the peak at the η mass coming from the decay chain $\phi \to \eta\gamma$,$\eta \to \gamma\gamma$. Under both peaks there is a big background. In the case of the η it is only due to the combinatorial background, that is when the photons 1-2 don't come both from the η decay but one of the from the ϕ decay.
This can be easily deduced by looking at fig.7. In fact being

$$m^2_{12} + m^2_{13} + m^2_{13} = m^2_{\phi},$$

the line that cross the center of the histogram is due to the cases when the photons 1-3 come from the η decay. In the π^0 case there is not misidentification background because the photons coming from the π^0 are always the least energetic ones. In the π^0 case the background is given by the $\eta \to 2\gamma$ sample and by the $e^+e^- \to \gamma\gamma$ with an acidental cluster that is evident in the upper part of the dalitz plot. The uncertainty on the background shape and the correlation betwwen the background parameters

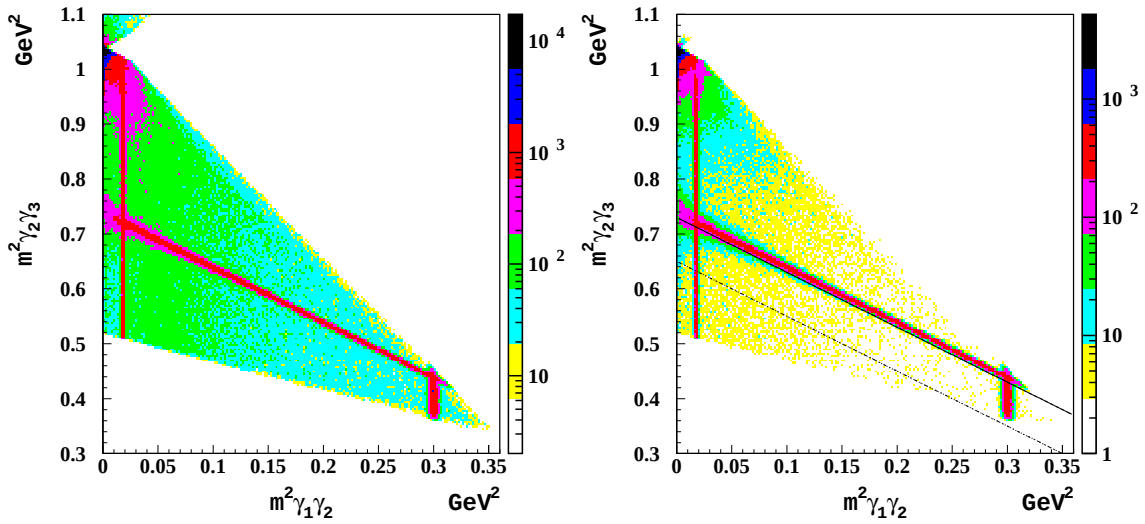

Figure 7: Dalitz plot distributions before (left) and after (right) the application of the $\chi^2 < 35$ cut.

fit results					
	χ^2_0/n.d.f	Prob($\chi^2 > \chi^2_0$)	m (MeV)	σ_1 (MeV)	σ_2 (MeV)
η	154/161	57 %	547.710 ± 0.014	2.14 ± 0.012	-
π^0	255/257	43 %	134.94 ± 0.02	1.78 ± 0.05	4.07 ± 0.19

Table 1: Fit parameters for the π^0 and η mass distribution. In the π^0 case the sigma of the two gaussians are shown.

and the central value of the peak, spoils the precision of the measurement. For this reason it is important to clean the sample as much as possible,

In fig.8 the distribution of $m_{\gamma 1 \gamma 2}$ is reported before (left) and after (right) the cut indicated with the continuous line in fig.7.

To determine the π^0 mass a stronger cut is needed in order to reduce the background at an optimum level (fig. 9), it is shown with the dashed line in fig. 7 (right). The peak at the η mass value of fig. 8 has been fitted with a gaussian distribution using a MINUIT fit procedure. The result of the fit has been reported in fig. 10 for 60 pb^{-1} in the run range 17874-20600, just as an example. While a double gaussian distribution is needed to reproduce the π^0 shape. The result of the fit are reported in table 1. It is possible to see that the statistical error using 60 pb^{-1} of data is about 14 keV (3×10^{-5}). The potential high precision of the measurement implies the needed of a carefull study of all systematic effects that could spoil this level of precision.

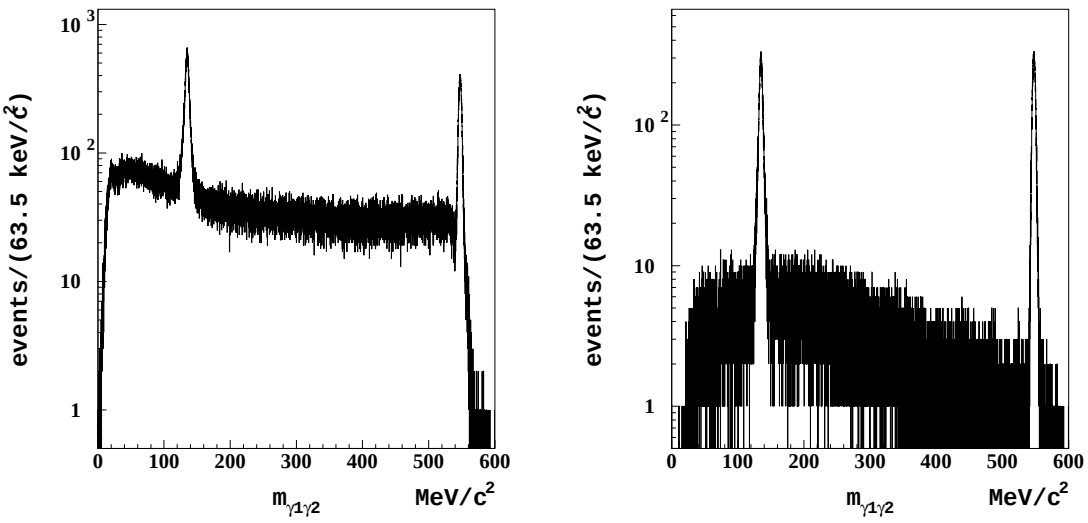

Figure 8: Invriant mass distribution, minimum energetic photons.

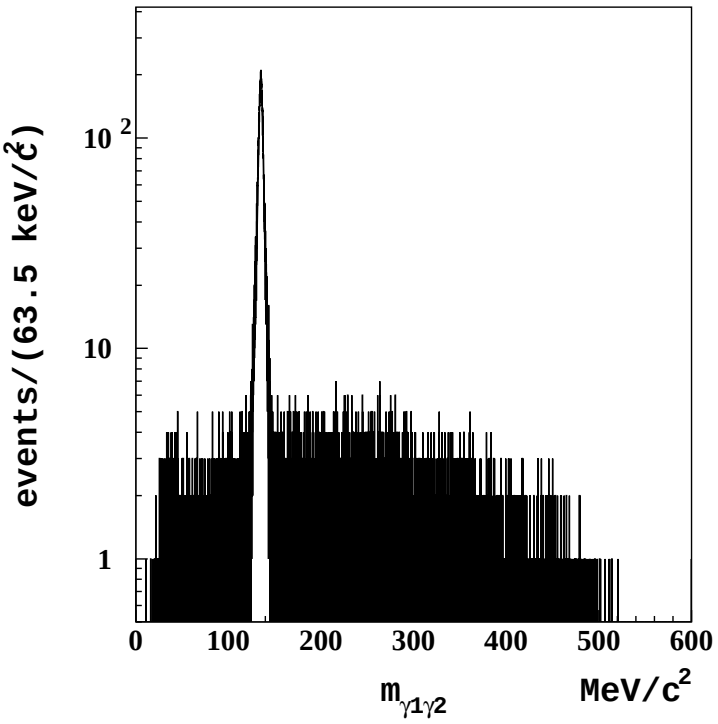

Figure 9: $m_{\gamma 1 \gamma 2}$ distribution for the π^0 selection.

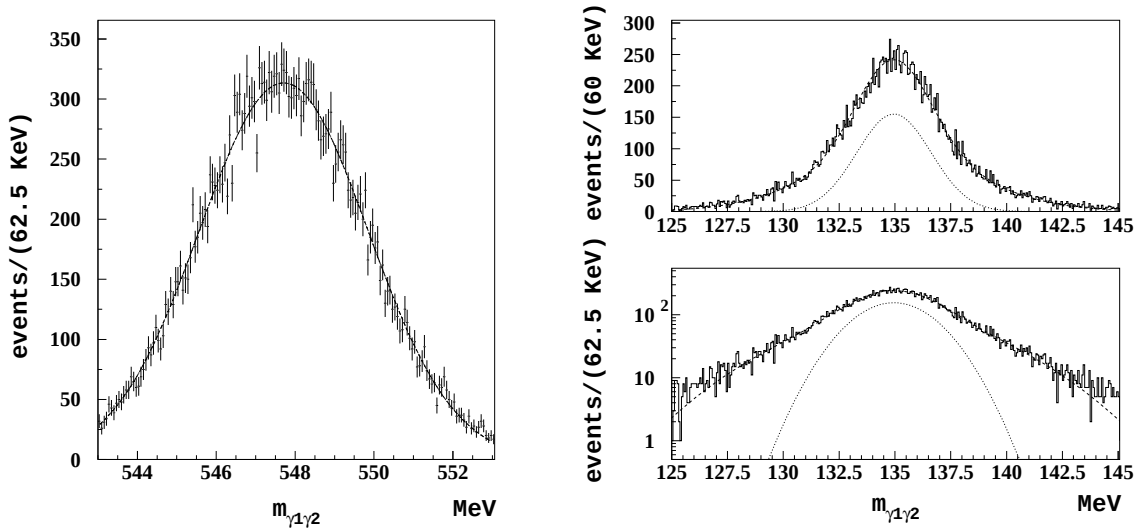

Figure 10: Invariant mass distribution for the $\eta \to \gamma\gamma$ decay (left) and for the $\pi^0\gamma\gamma$ decay (right). The fitted function are shown. The small gaussian in the π^0 case is the core gaussian.

4 Systematic error evaluation.

The sources of systematic error against several effects has been studied. The effects considered are: calorimeter absolute energy calibration, energy response non linearity, cluster position calibration and non linearity in ϕ and z coordinate, mean interaction vertex knowledge, $\sqrt{s}$ knowledge, χ^2 cut effect, angular cut effect, global disallineament between the Drift Chamber and the calorimeter. To evaluate the systematic effect we have used the π^+,π^-,γ sample used in the hadronic cross section measurement at large angle. This sample is used to estimate systematic on vertex position determination, ϕ, z and E global calibration and non-linearity, global disallineament between the Drift Chamber and the calorimeter.

4.1 Vertex position systematic evaluation.

The vertex position is determined run by run by the physmon program using bhabha events. To evaluate a systematic on this measurement we use the vertex position reconstructed in the π^+ π^- γ sample. The 2001 data period has been divided into ... pb$^-$1 of runs. for eac group of run the quantity $(X_{\pi\pi\gamma} - X_{BPOS})$, $(Y_{\pi\ pi\gamma} - Y_{BPOS})$, $(Z_{\pi\pi\gamma} - Z_{BPOS})$ are put in an histogram. The fit to a double gaussian with the same mean should give a mean value of zero if any not common systematic between the bhabha sample and the $\pi^+\pi^-\gamma$ sample is seen.

In fig. 11 we report the mean of the two gaussian as a function of the run number at the beginning of the run bunches for 2001 and 2002 data taking. The uncertainity

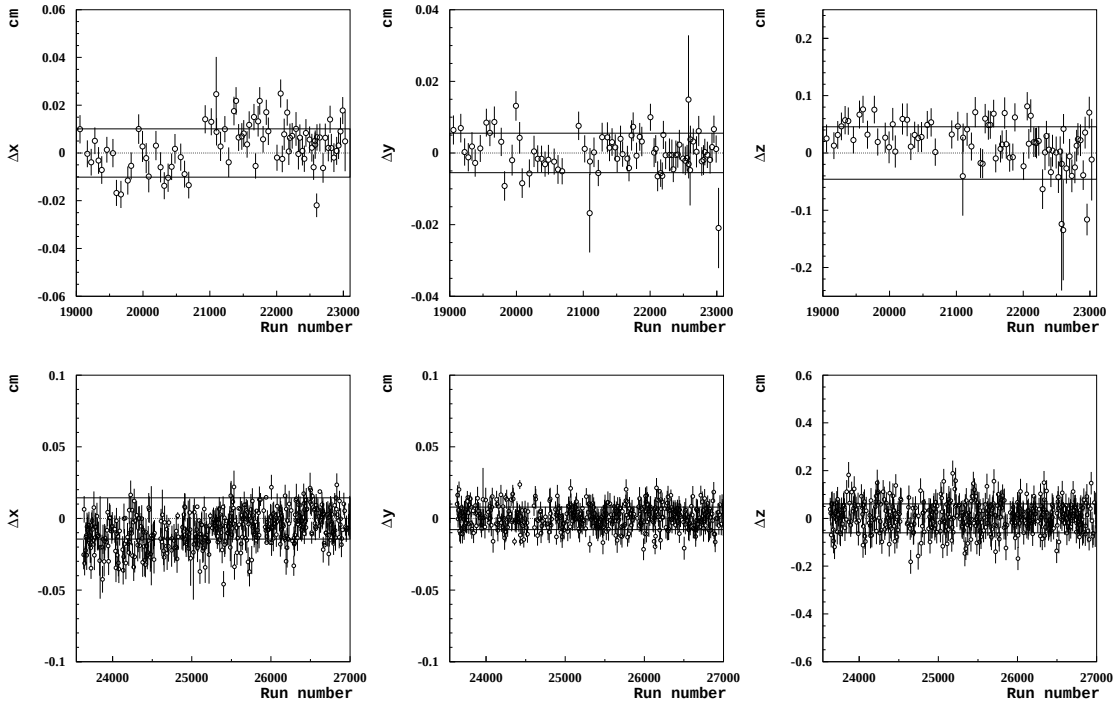

Figure 11: Distribution of the difference in the vertex position between the $\pi^+\pi^-\gamma$ sample and the $BPOS$ value. Top 2001 DATA, bottom 2002 DATA.

Systematic due to the vertex position (cm).							
	2001			2002			
coord.	rms I.P	DC-calo al. π^+	DC-calo al. π^-	rms I.P	DC-calo al. π^+	DC-calo al. π^-	tot. syst.
x	0.010	0.04	0.034	0.014	0.062	0.056	0.056
y	0.006	0.12	0.08	0.008	0.13	0.088	0.088
z	0.046	0.16	0.17	0.061	0.22	0.28	0.22

Table 2: Corrections to the vertex position and associated systematic error.

due to the vertex position is estimated by evaluating the rms of these points respect to the expected value of zero. The rms is asssumed as the systematic associated to this determination. In tab. 2 these errors are shown.

A possible common systematic between the $\pi\pi\gamma$ sample and the bhabha one can be due to a possoible displacement, not corrected in the reconstruction, between the calorimeter respect to the drift chamber. The vertex measured by with the charged track is of course linked to the drift chamber reference frame. In order to check the DC-calorimeter allineament we use the extrapolation of the tracks of the $\pi^+\pi^-\gamma$ sample to the calorimeter. The tracks are extrapolated from the vertex in the DC to the calorimeter assuming a constant magnetic field of $0.5188T$ along the z direction. The point of nearest approach to the cluster centroid is computed, where the cluster is that associated by the track to cluster algorithm. Any displacement between the DC and the barrel can be evaluated by studing the distribution of the residuals $X_{clu} - X_{extr}$, $Y_{clu} - Y_{extr}$, $Z_{clu} - Z_{extr}$. The average of the residuals on several group of runs are plotted as a function of the first run of the period in fig.13 for the 2001 and 2002 data taking. As one can see, while the x position is well centered the y position has is shifted of about 1 mm while the z position has a time behaviour as a function of the run number. For the pourpose of this work we don't apply any correction and estimate just a systematic error on this distribution. The systematic error is evaluated as the standard deviation respect to the expected value, 0, of all the distributions shown in the plot. The values are reported in tab. 2.
Both the uncertainity on the vertex position and the displacement between the calorimeter and the drift chamber have the same effect on the measurement. They change the angle between the two photons coming from the η decay and so they have to be accounted together. The two effect are completely uncorrelated, so we sum in quadrature this effects. Between the π^+ and π^- data we take the smallest one, in fact any increment can only be due to the particle type and so to the method used to evaluate the displacement and not to the real knowledge of the displacement. To be conservative for the DC-Calo alineament systematuc we take the values of 2002 because the uncertainty is higher. The cumulative effect is evaluated in the last column of tab. 2. To evaluate the effect of these uncertainties on the value of the η mass we proceed in the following way: we apply run by run a systematic shift of 1

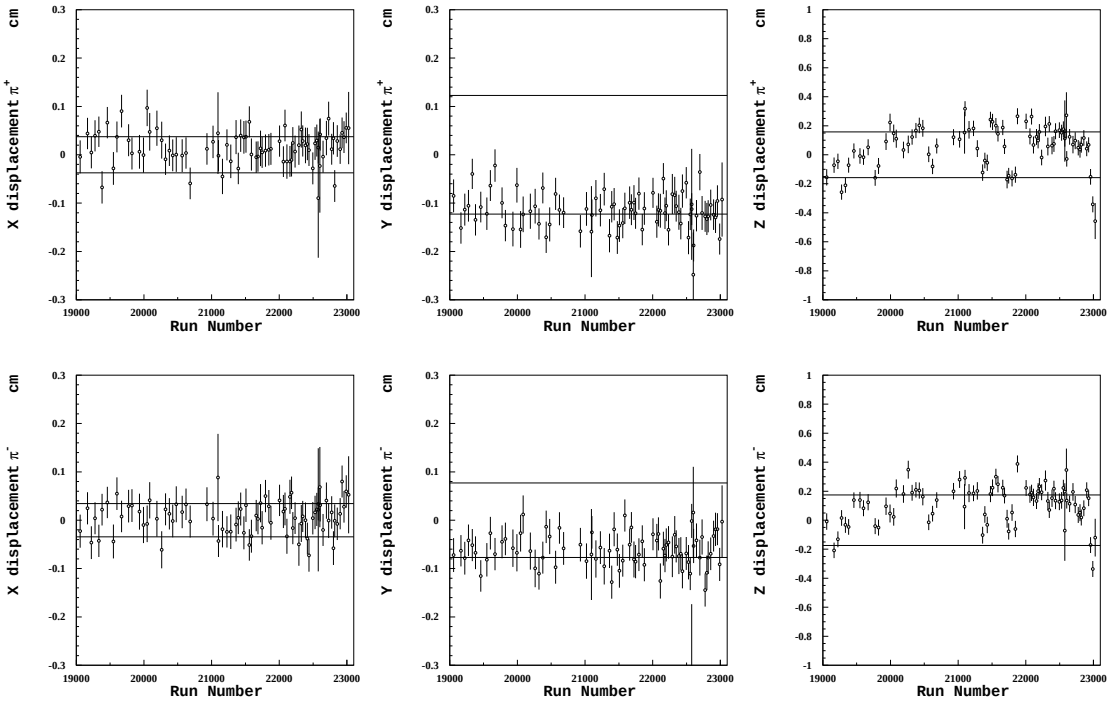

Figure 12: Mean of the residuals of the extrapolated track position respect the cluster centroid for π^+ and π^- in the year 2001.

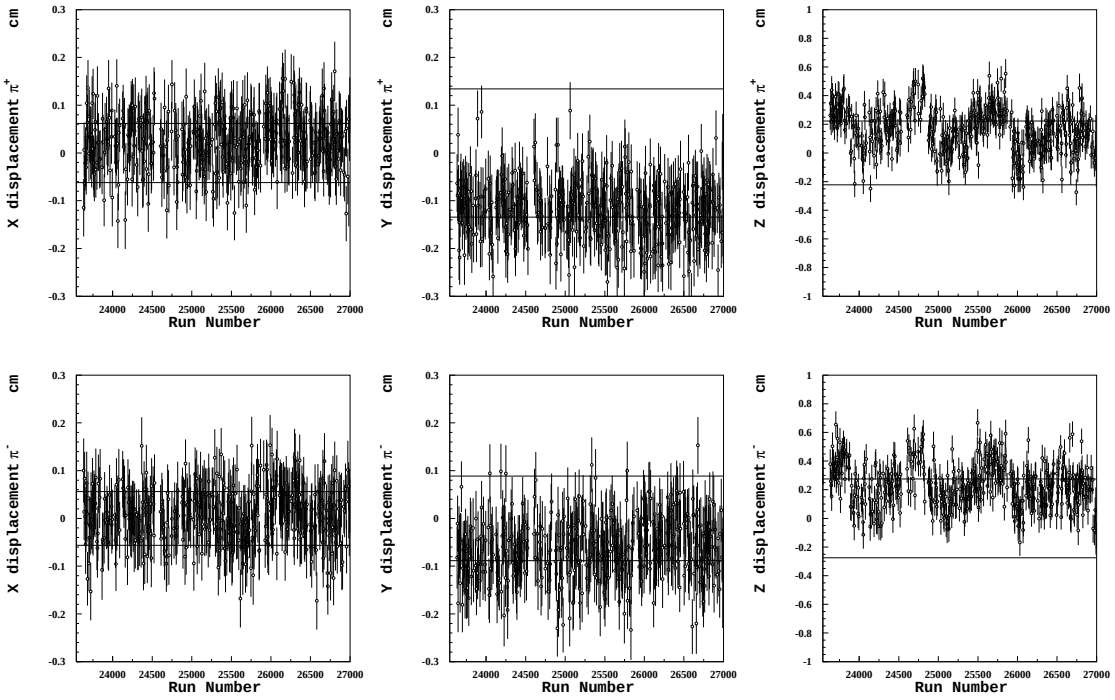

Figure 13: Mean of the residuals of the extrapolated track position respect the cluster centroid for π^+ and π^- in the year 2002.

	m_η $(\times 10^{-6})$	m_π $(\times 10^{-6})$	m_η/m_π $(\times 10^{-6})$
V_X	1.8	15	15
V_Y	7	22	27
V_Z	4	37	35
overall	8	45	47

Table 3: Fractional systematic error for different quantities related to the η mass measurement.

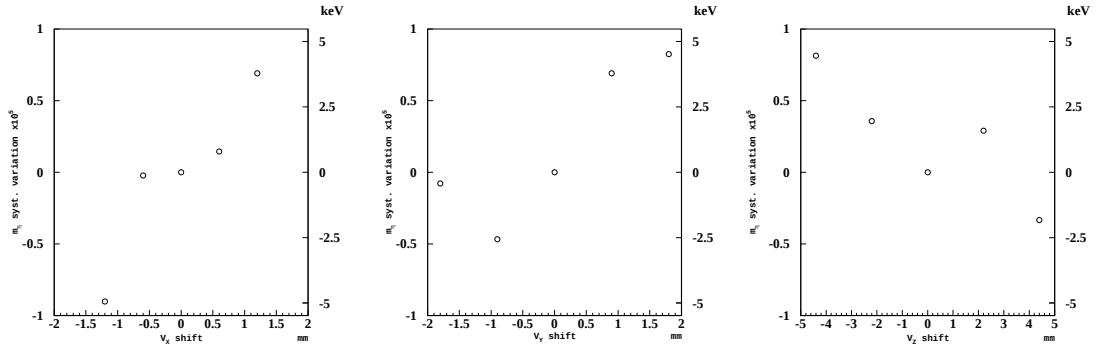

Figure 14: The η mass fractional shift as a function of the vertex position shift.

σ on the vertex position as evaluated on 2002 DATA. This because the 2002 DATA present a larger systematic error. We repeat the analysis and exstract the value of the η mass. The difference respect to the central value gives the upper and lower 1 σ systematic error. In fig. 16 we report the shift of the η mass as a function of the shift on the vertex position. From this figure we extract the contribute to the systematic error for the π^0, the η mass and the ratio m_{π^0}/m_η. The value obtained are shown in tab. 3

4.2 Energy linearity.

To estabilish a systematic error on the knowledge of the linearity response of the calorimeter, we use the $\pi^+\pi^-\gamma$ sample. For this pourpose we evaluate the missing energy from the $\sqrt{s}$ and the two charged pions momenta and we compare it with the energy of the prompt clusters in the calorimeter (the prompt cluster definition has been given in sec. **??**). In fig. 17 the scatter plot od the cluster energy as a function of the missing energy has been shown. It is evident the presence of two regions, one is the "linerity" region, that is the region used to evaluate the linearity, the other one is given by clusters with small energies, that is accidental clusters or splitted clusters. The two regions are well separated, so the simple cut shown in the figure is able to give a clean sample for linearity studies. The study has been done merging the whole 2001 and 2002 statistic, the two samples have been study

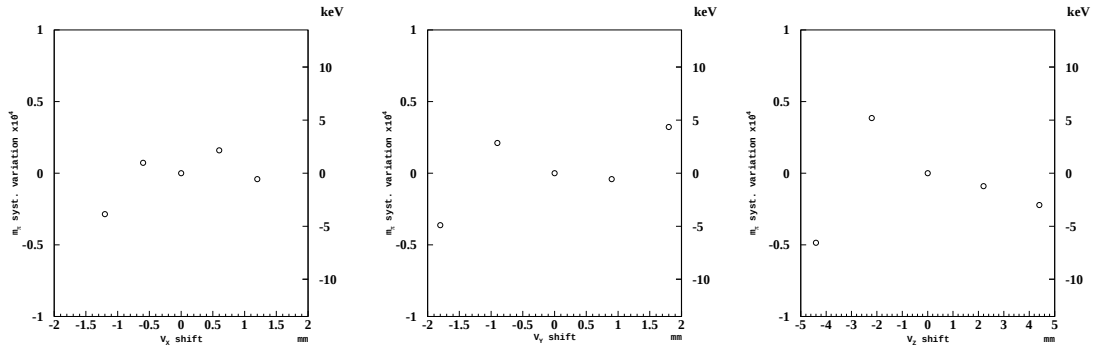

Figure 15: The π^0 mass fractional shift as a function of the vertex position shift.

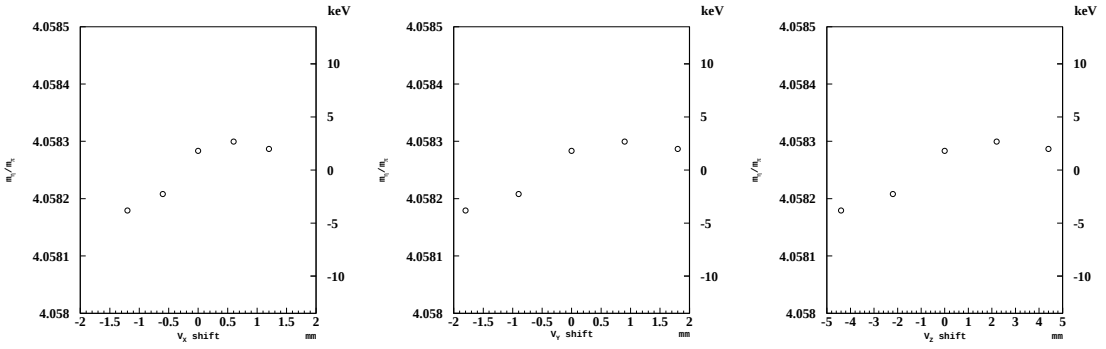

Figure 16: The $m(\eta)/m(\pi^0)$ ratio as a function of the vertex position shift.

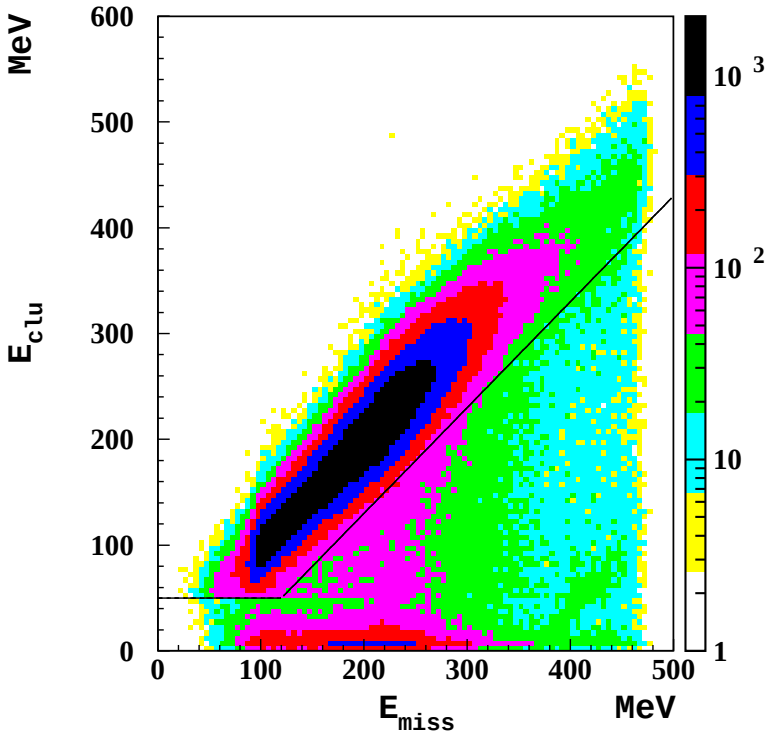

Figure 17: Scatter plot of the prompt cluster energy E_{clu} versus the missing energy of the π^+,π^-,γ events.

in indipendent way also but no difference has been observed.

The two dimensional histograms shown in fig.17 are sliced for energy regions of ... MeV. Each slice is fit with a gaussian distribution and the mean value and the error are used to estimate the systematic. In fig. 18 the linearity curve is shown for 2001 and 2002 data. The curve is fit using a linear approximation $E_{clu} = a + b \cdot E_{miss}$, the value of a and b are shown in table 4.

To study the calorimeter non linearity we proceed in the following way. We build the quantity:

$$\frac{E_{clu} - (a + b * E_{true})}{E_{true}} \approx \frac{E_{clu} - (a + b * E_{miss})}{E_{miss}} \quad (1)$$

Linearity response parameters				
a (MeV)	b	c	d (MeV^{-1})	e (MeV^{-2})
-0.2	0.994	-2.1	0.019	-4.2×10^{-5}

Table 4: Fitted parameters of the linearity curve.

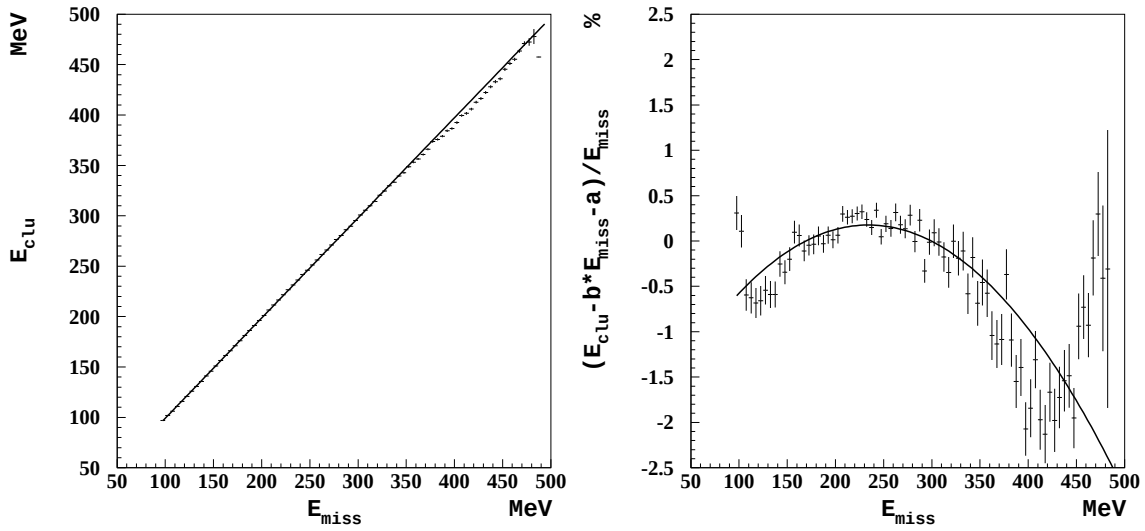

Figure 18: **left** Linearity response, the fit function is overimposed; **right** Fractional alinearity according the formula (1). The value of the parameters are shown in tab. 4.

this quantity is exactly 0 for a perfect linearity response. Small alinearity can be considered by parametrizing the deviation from zero of this quantity as:

$$\frac{E_{clu} - (a + b * E_{miss})}{E_{miss}} = c + d * E_{miss} + e * E_{miss}^2 \tag{2}$$

This take into account a possible quadratic and cubic term in the energy response. The value of c, d, e are used to parametrize the alinearities. In fig. **??** we show the quantity (1) for the $\pi^+\pi^-\gamma$ sample together with a fit to a second order polynomial. The alinearity at 2% level shown in figure, can be, in principle, due to the chosen control sample, such as the presence of $\pi^+, \pi^-\pi^0$ contamination or two photons processes. Anyway, for the puorpose of this study, we can conservative assume that the shown alinearity is due to the real alinearity of the calorimeter and use the alinearity curve to estimate a systematic effect on the η mass value.
Applying the linearity coefficient of table 4 the result of the mass shift of 8×10^{-6}, this value is assumed as systematic error, while applying the coefficients on the alinearity the shift is of 7×10^{-6}.

5 Systematic checks.

Other systematic effect can be due to the not uniformity of the calorimeter response for the cluster position determination. To check this effect we evaluate the η mass as a function of the azimutal and polar angle of a vector orthogonal to the 3γ plane.

This vector is determined using the vector product between the two most energetic photon momenta.

References

[1] A. Duane et al., Phys. Rev. Lett. 32, 425 (1974)

[2] F. Plouin et al, Phys. Lett. B 276 (1992) 526

[3] A. Lai et al., Phys. Lett. B 533 (2002) 196.

[4] M. Abdel-Bary et al., Phys. Lett. B 619 (2005) 281

[5] B. Krusche et al., Z. Phys. A 351, 237

[6] http://www.isv.uu.se/etamesonnet/news.php (go to internal pages: login etameson password: network)

[7] S. Eidelmann et al., Phys. Lett. B 592 (2004) 1

[8] B. Di Micco, KLOE memo n. 282, (2004);

[9] S. Dell'Agnello, M. Primavera, KLOE memo n. 202, (2000)

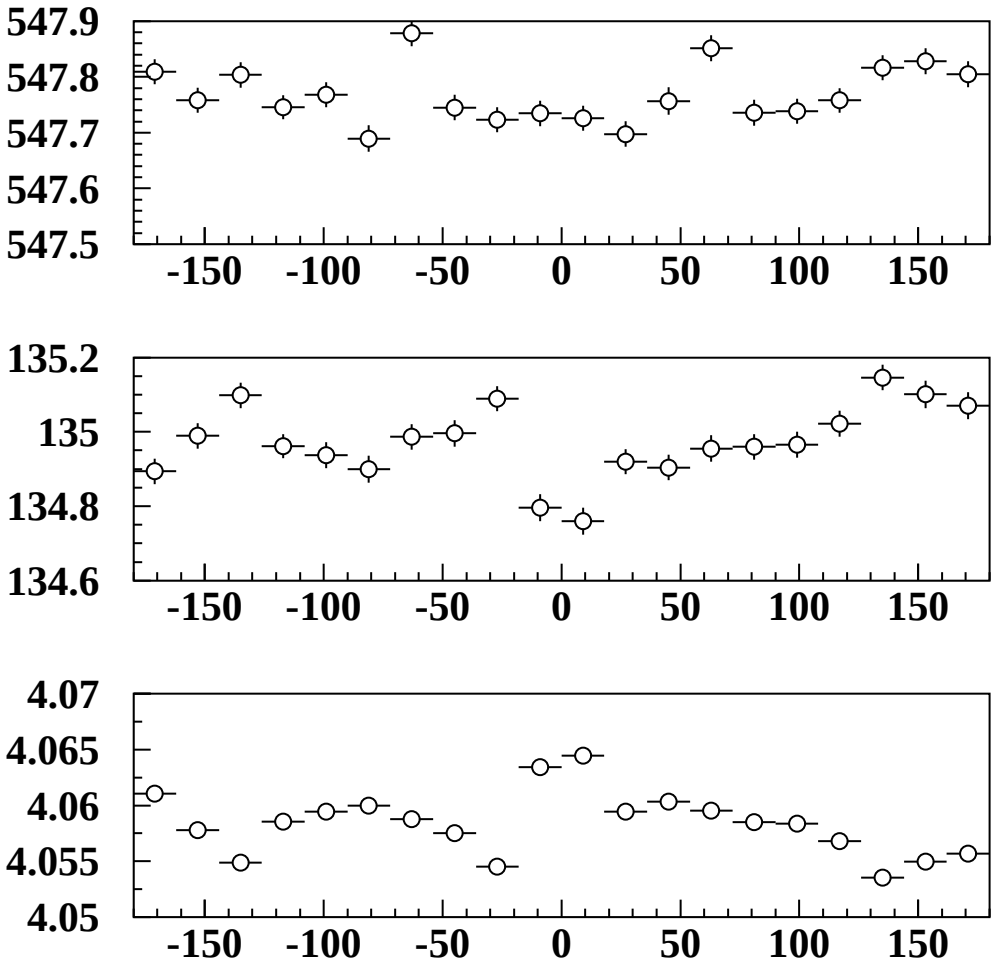

Figure 19: Azimuthal angle.

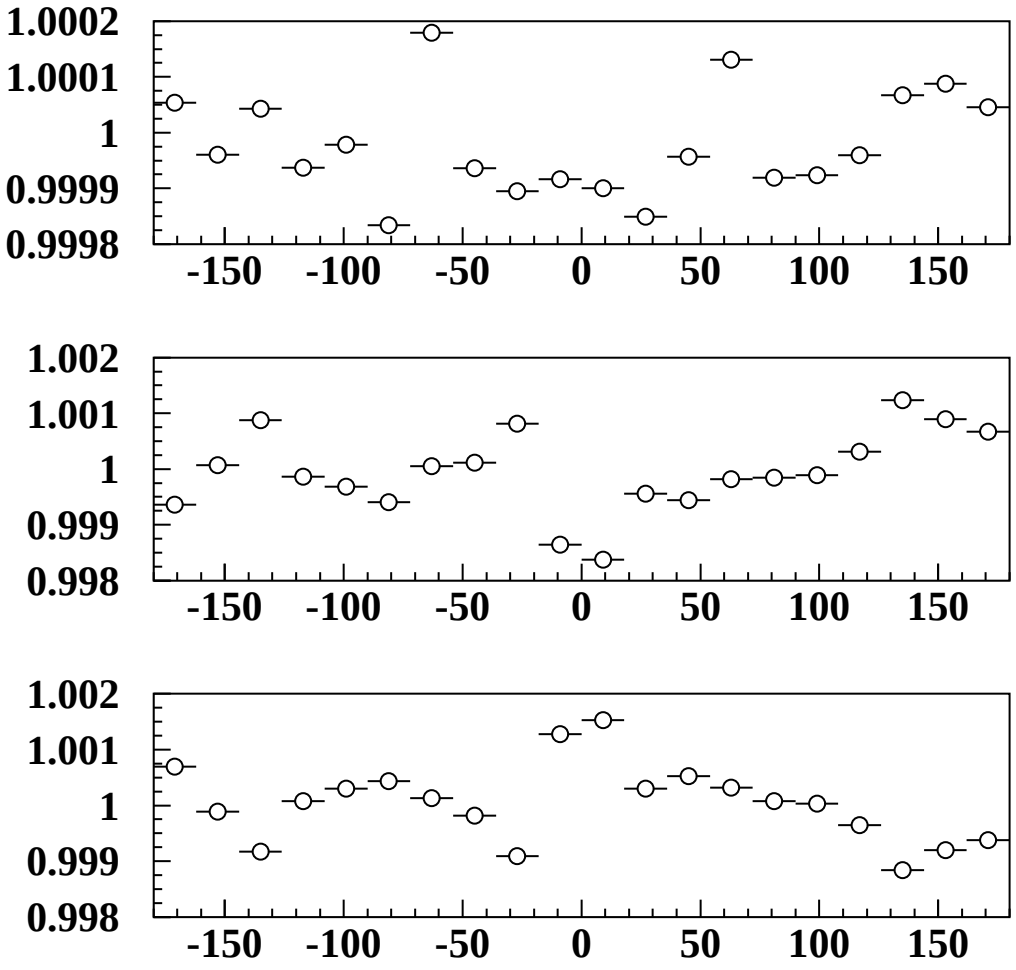

Figure 20: Azimuthal angle.

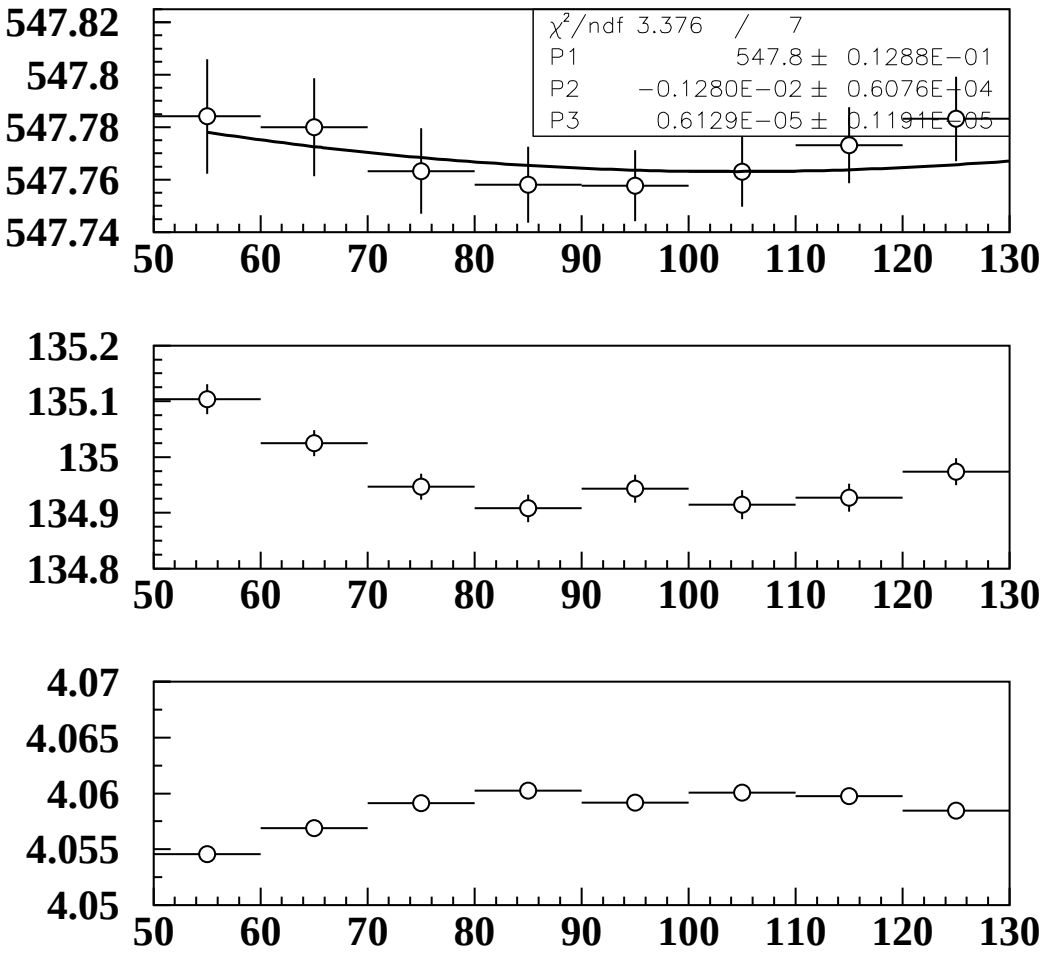

Figure 21: Polar angle.

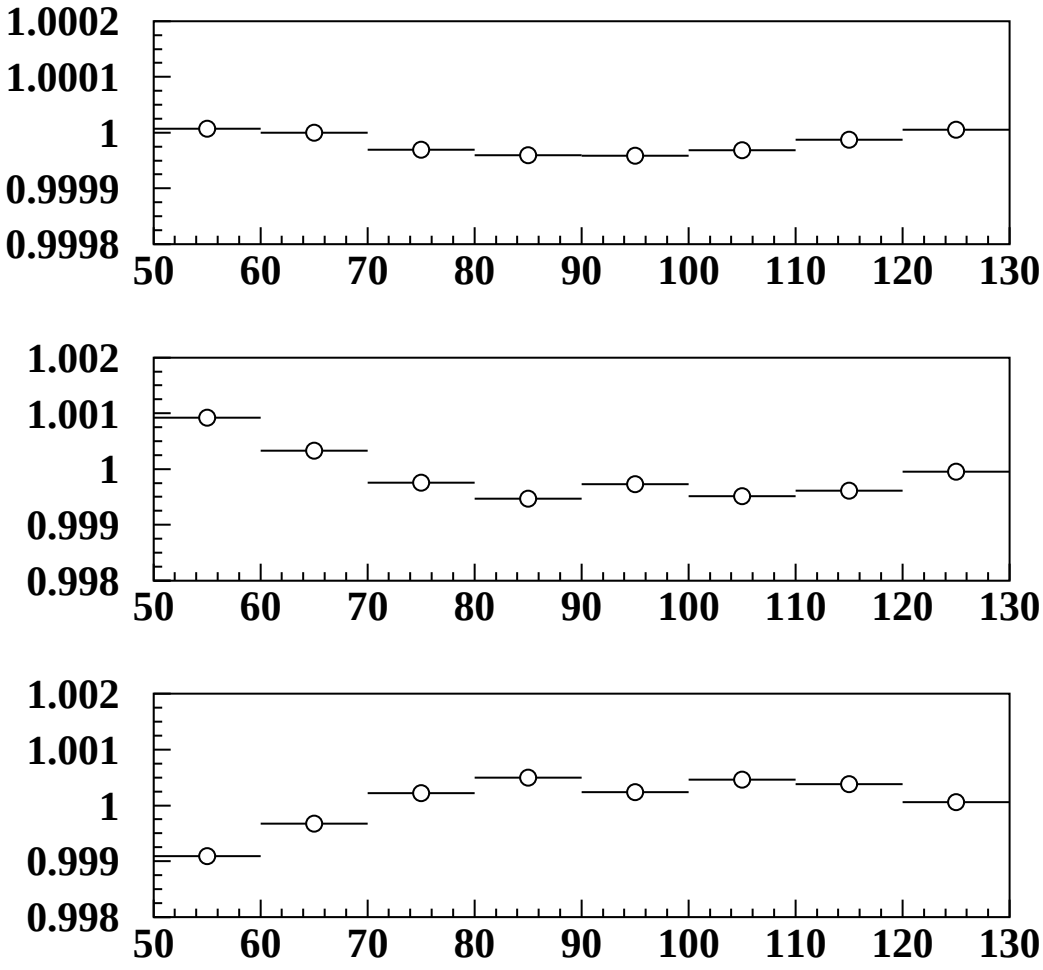

Figure 22: Polar angle.